Viscous photons in relativistic heavy ion collisions

Maxime Dion, Jean-François Paquet, Björn Schenke, Clint Young, Sangyong Jeon, and Charles Gale

Viscous photons in relativistic heavy ion collisions

Maxime Dion,[1] Jean-François Paquet,[1] Björn Schenke,[2] Clint Young,[1] Sangyong Jeon,[1] and Charles Gale[1]

[1] Department of Physics, McGill University, 3600 University Street, Montreal, Quebec, H3A 2T8, Canada

[2] Physics Department, Bldg. 510A, Brookhaven National Laboratory, Upton, NY 11973, USA

Theoretical studies of the production of real thermal photons in relativistic heavy ion collisions at the Relativistic Heavy Ion Collider (RHIC) are performed. The space-time evolution of the colliding system is modelled using MUSIC, a 3+1D relativistic hydrodynamic simulation, using both its ideal and viscous versions. The inclusive spectrum and its azimuthal angular anisotropy are studied separately, and the relative contributions of the different photon sources are highlighted. It is shown that the photon v_2 coefficient is especially sensitive to the details of the microscopic dynamics like the equation of state, the ratio of shear viscosity over entropy density, η/s, and to the morphology of the initial state.

I. INTRODUCTION

The study of relativistic collisions of nuclei constitutes a vibrant branch of subatomic physics that straddles nuclear and particle physics. It offers a privileged window on the physics of hot and dense strongly interacting matter and as such, it complements astrophysical studies. There, the hadronic equation of state is an ingredient of paramount importance that enters the evaluation of the bulk properties of neutron stars, for example. In comparison, relativistic nuclear collisions do offer the considerable practical advantage of providing laboratory control over the projectile and target characteristics, together with the beam energy. This physics currently defines a large experimental effort being pursued at the Relativistic Heavy Ion Collider (RHIC), at Brookhaven National Laboratory and, more recently, at the Large Hadron Collider (LHC), at CERN. One of the remarkable results that emerged from the RHIC program so far, is the fact that the hot and dense hadronic matter produced there [1–4] could be described using almost ideal hydrodynamics, that is with a small shear viscosity coefficient η [5], compared to the entropy density s. The first LHC flow results for heavy ion collisions [6] also suggest similar conclusions: a recent overview of flow results can be found in Ref. [7]. In fact, the progress in both theoretical and in experimental analyses has been such that the goal of a quantitative extraction of the shear viscosity coefficient of hot and dense strongly interacting matter from relativistic nuclear collision data now appears closer than ever [8–13].

In heavy-ion collisions, the flow has been characterized by considering a Fourier expansion of the the triple differential cross-section, with the variable being the azimuthal angle with respect to the reaction plane [14]:

$$E\frac{d^3N}{d^3p} = \frac{1}{2\pi}\frac{d^2N}{p_T dp_T dy}\left(1 + \sum_{n=1}^{\infty} 2v_n \cos\left[n\left(\phi - \psi_r\right)\right]\right)$$

(1)

where ψ_r is the reaction plane angle. The expansion coefficients, v_n, will then quantify the degree of azimuthal anisotropy. In the progress towards a precise and quantitative characterization of the hydrodynamical state of nuclear collisions, a recent development consisted of linking the odd-numbered coefficients to fluctuations in the initial state [15]. Indeed, up to this point the flow observables in nuclear collisions had been analyzed by considering the coefficients of the Fourier expansion of the azimuthal angle distribution of the particle spectra, together with smooth initial conditions for which the odd values of the Fourier coefficients vanish [14]. It is fair to write that a rich and quantitative picture of nuclear flow is now emerging[1].

In general, the measured hadronic observables give a dynamical snapshot of the conditions that existed on the freeze-out hypersurface. In contrast, electromagnetic radiation is emitted throughout the space-time evolution and suffers negligible final-state interactions, owing mainly to the smallness of α, the electromagnetic coupling constant. Real and virtual photons are thus penetrating probes, and as such can carry information about the different stages of the high energy collisions. A consequence of this statement is that accurate and meaningful calculations of photon spectra in relativistic nuclear collisions will need realistic electromagnetic emissivities and precise modelling of the space-time dynamics. The goal in this paper is to extend the calculations of real photon production to situations which incorporate the developments made on the purely hadronic front. Cases where the emitting source is no longer in local thermal equilibrium will be considered, together with cases where the initial states of the nucleus-nucleus

---

[1] A discussion on how to calculate the elliptic flow, v_2, in the presence of fluctuating initial conditions appears later in this paper.

collisions are no longer smooth but are allowed to fluctuate event-by-event. The paper is organized as follows: section II contains a brief description of MUSIC, our implementation of 3+1 viscous hydrodynamics which is used to calculate the evolution of the background medium. In section III, we give a short explanation of viscous corrections to the local momentum distribution function and the photon emission rates used in this study. Our main results are presented in section IV and we conclude in section V.

II.   HYDRODYNAMICAL EVOLUTION

As mentioned earlier, photons are penetrating probes that are emitted throughout the heavy-ion collision. It is thus imperative to evaluate their observed properties with a time-evolution scenario that is both realistic and consistent with a large number of empirical observables. One such approach is MUSIC, a three-dimensional simulation of relativistic hydrodynamic systems [16]. The general features of MUSIC are described below, first in the ideal limit, and then incorporating a finite coefficient of shear viscosity.

The solution of the conservation laws for the stress-energy tensor and the net baryon current, $T^{\mu\nu}$ and J_B^μ, respectively, dictate the evolution in time of an ideal hydrodynamical system. More specifically,

$$\partial_\mu T^{\mu\nu}_{\text{ideal}} = 0\,,$$
$$\partial_\mu J^\mu_{\text{B,ideal}} = 0 \tag{2}$$

and

$$T^{\mu\nu}_{\text{ideal}} = (\epsilon + P)\, u^\mu u^\nu - P g^{\mu\nu}\,,$$
$$J^\mu_{\text{B,ideal}} = \rho_B u^\mu \tag{3}$$

Note that P is the local pressure, ϵ is the local energy density, ρ_B is the local net baryon density, $u^\mu = (\gamma, \gamma\mathbf{v})$ is the local flow velocity with respect to some fixed frame, and $g^{\mu\nu} = \text{diag}\,(1, -1, -1, -1)$. This represents a set of five scalar equations, with six unknowns. The set is closed by specifying an equation of state, $P(\epsilon, \rho_B)$. MUSIC is implemented in $\tau - \eta_s$ coordinates, where τ is the proper time, and η_s the space-time rapidity. The transformations to real time and longitudinal coordinate variables, $\{t, z\}$, are

$$t = \tau \cosh \eta_s\,, \quad z = \tau \sinh \eta_s \tag{4}$$

The solution of Eqs. (2) in $\tau - \eta_s$ coordinates is obtained with the Kurganov-Tadmor method [17], and an equation of state extracted from lattice QCD calculations [18] is used in this work. Importantly, MUSIC is a three-dimensional simulation, and is therefore capable of following the time evolution of the rapidity profile. It has been used for the successful calculation of flow variables, including elliptic flow and higher flow harmonics [16]. A discussion of results with ideal hydrodynamics is postponed, turning now to the inclusion of viscous effects.

The first-order - or Navier-Stokes - formalism for viscous hydrodynamics is known to introduce unphysical superluminal signals that spoil the theory's stability. Various formulations of second-order hydrodynamics [19–23] address this problem, and a variant [24] of the Israel-Stewart formalism is used here. In this approach, the stress-energy tensor is $T^{\mu\nu} = T^{\mu\nu}_{\text{ideal}} + \pi^{\mu\nu}$, and the evolution equation are

$$\partial_\mu T^{\mu\nu} = 0\,,$$
$$\Delta^\mu_\alpha \Delta^\nu_\beta u^\sigma \partial_\sigma \pi^{\alpha\beta} = -\frac{1}{\tau_\pi} \left(\pi^{\mu\nu} - S^{\mu\nu} \right) - \frac{4}{3} \pi^{\mu\nu} \left(\partial_\alpha u^\alpha \right)$$

$$\tag{5}$$

where $\Delta^{\mu\nu} = g^{\mu\nu} - u^\mu u^\nu$, and τ_π is usually interpreted as a relaxation time . The first-order (in velocity gradients) viscous part of the stress-energy tensor appears here and is

$$S^{\mu\nu} = \eta \left(\Delta^\mu u^\nu + \Delta^\nu u^\mu - \frac{2}{3} \Delta^{\mu\nu} \nabla_\alpha u^\alpha \right)\,, \tag{6}$$

with the coefficient of shear viscosity η, and $\nabla^\mu = \Delta^{\mu\nu} \partial_\nu$. The viscous stress-energy tensor $\pi^{\mu\nu}$ is clearly a complicated object that is evaluated dynamically. Finally, vorticity and numerically small terms have been neglected.

Hydrodynamic calculations require their initial states to be defined. In this work, smooth or averaged initial conditions (AIC) will be considered, as well as cases where these initial states are allowed to fluctuate (FIC) about that average. The procedure for implementing AICs in MUSIC is described in detail in Ref. [16], and that for FICs, in Ref. [9]; those descriptions will not be repeated here. The initial time for the hydro to start is defined by τ_0, in

this work this value is set to $\tau_0 = 0.2$ fm/c, and the freeze-out energy density is 0.12 GeV/fm^3, which approximately corresponds to T = 137 MeV.

Considering first AICs, it is instructive to study how the inclusion of shear viscosity affects the bulk evolution. The physical case being considered is that of Au + Au, at $\sqrt{s} = 200$ GeV, at an impact parameter of $b = 4.47$ fm, which represents a 0 - 20 % centrality class. As mentioned earlier, the equation of state used here is the parametrization "s95p-v1" from Ref. [18]. In this parametrization, the fit to the lattice QCD data is made above $T = 250$ MeV with the constraint that at $T = 800$ MeV, the energy density reaches 95 % of the Stefan-Boltzmann value. It is also worth noting that this parameterization correctly reproduces the trace anomaly around the transition temperature: see Ref. [18] for more details.

Figure 1 shows the evolution of temperature for a fixed cell at $x = y = 2.5$ fm and $z = 0$. In the case with a non-zero
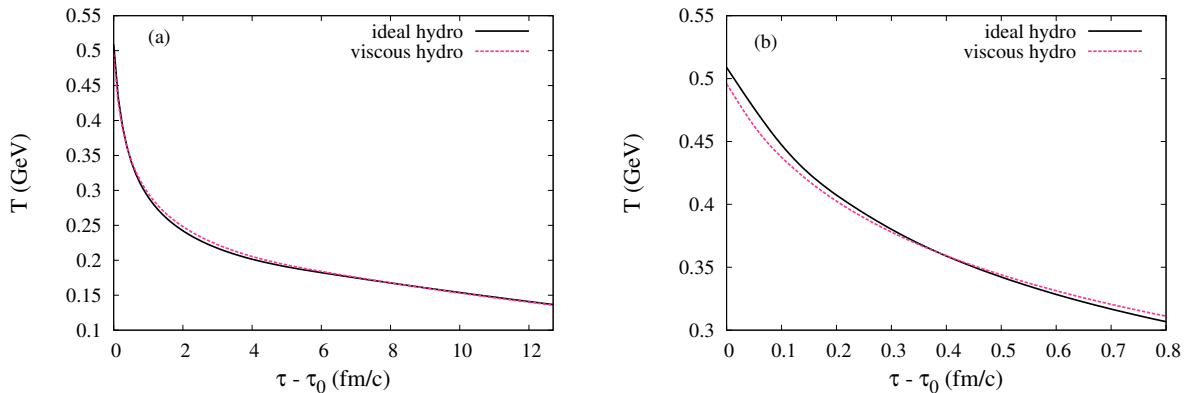

FIG. 1. (Color online) Left panel: The evolution of temperature in a fixed cell, as a function of time. Results for ideal and viscous hydrodynamics (with $\eta/s = 1/4\pi$) are shown. Right panel: A closer view of the early time temperature evolution.

shear viscosity, a value of η/s (the shear viscosity divided by the entropy density) $= 1/4\pi$ has been used. This value has been suggested as a lower universal bound [25], a statement which has raised some controversy and thus needed to be qualified [26–28]. Furthermore, η/s will also depend on the local temperature of the medium, but a constant value will suffice for the study in this work. Note that the finite viscosity calculation has a smaller initial temperature than the ideal one, as entropy will grow in the viscous case, affecting the observed final particle multiplicity: it is important to compare calculations consistent with a given set of hadronic observables.

III. PHOTON EMISSION FROM IDEAL AND VISCOUS MEDIA

Viscous corrections on microscopic processes involving particles have been included by writing the in-medium distribution functions with an out-of-equilibrium correction, $f_0 \rightarrow f_0 + \delta f$, where f_0 is an ideal Bose-Einstein/Fermi-Dirac distribution function. This is most easily seen by considering the particle spectra being generated from the Cooper-Frye formalism [29], and requiring that the energy momentum tensor be continuous across the freeze-out hypersurface. In a multispecies ensemble, a popular ansatz that satisfies the continuity requirements is

$$\delta f_i = f_{0i} \left(1 \pm f_{0i}\right) p^\alpha p^\beta \pi_{\alpha\beta} \frac{1}{2\left(\epsilon + P\right) T^2} \tag{7}$$

for the distribution function of species i. This form is used in this work. In general, there can be an overall constant, different for each species, that multiplies Eq. (7) [30]. It is implicit in this treatment that δf should represent a small correction. In the calculation of pions and of other hadronic observables, one simply needs to verify this statement on the freeze-out hypersurface. This is not the case for electromagnetic emission which occurs at all time-scales of the hydro evolution. Therefore, photon calculations in viscous media will represent a stringent test of the validity of the viscous dynamics, as shall be seen later.
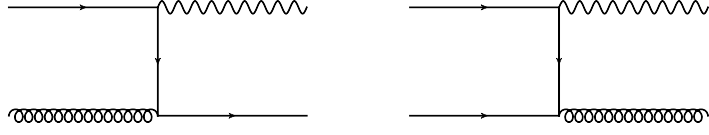
FIG. 2. The Compton and quark-antiquark annihilation contributions to photon production.

A. Photon emission from the QGP

Rates, complete at leading order in α_s, for the emission of photons from a thermal ensemble of partons have now been available for a decade [31]. The extension of these results to viscous media necessitates revisiting the resummation procedure in Ref. [31] with out-of-equilibrium distributions: a process we shall not perform here. We rather concentrate on a subset of the diagrams: the Compton and quark-antiquark annihilation processes shown in Figure 2. It is instructive to compare the photon rate obtained through the approach described above with the complete result at leading order in α_s: this is done in Fig. 3. At low p_T, the full leading order rates are an order of magnitude larger than the naive leading order rates owing to additional processes. For examples, the former receive a large contribution of brehmsstrahlung from quarks of all momenta in this range. For $p_T > 1$ GeV, the full leading order rates are only larger by about a factor of two (there is however some temperature dependence to the position of this transition window).
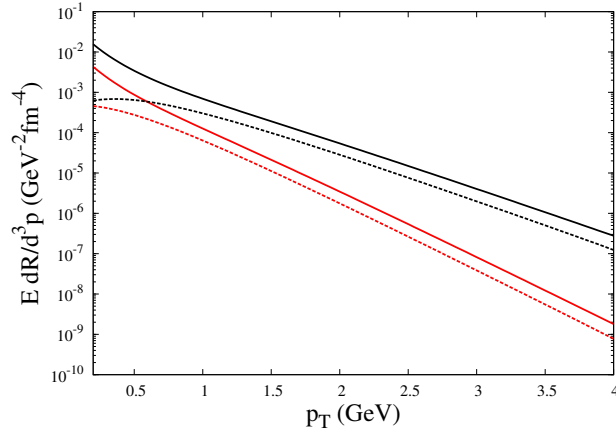

FIG. 3. (Color online) A comparison of the equilibrium photon rate from the processes shown in Figure 2 (dashed lines) with that obtained tallying all channels contributing at leading order in α_s (full lines), for $N_f = 3$. The lower set of curves are for T = 250 MeV, and the upper ones are for T = 350 MeV.

The net photon emission rate R, summing these individual processes of the type $1 + 2 \rightarrow 3 + \gamma$, is obtained by evaluating

$$E\frac{d^3R}{d^3p} = \sum_i \frac{\mathcal{N}}{(2\pi)^7} \frac{1}{16E} \int dsdt |\overline{\mathcal{M}}_i|^2 \int dE_1 dE_2 f_1(E_1) f_2(E_2)$$

$$\times \left[1 \pm f_3(E_1 + E_2 - E)\right] \frac{\theta\left(E_1 + E_2 - E\right)}{\sqrt{(aE_1^2 + bE_1 + c)}} \tag{8}$$

where the coefficients a, b, c are defined in Eq. (A.11), and where $|\overline{\mathcal{M}}_i|^2 = 16\pi s^2 d\sigma_i/dt$, with

$$\frac{d\sigma_{\text{annihil.}}}{dt} = \frac{8\pi\alpha\alpha_s}{9s^2} \frac{u^2 + t^2}{ut},$$

$$\frac{d\sigma_{\text{Compt.}}}{dt} = \frac{-\pi\alpha\alpha_s}{3s^2} \frac{u^2 + s^2}{us} \tag{9}$$

Note also the degeneracy factors $\mathcal{N}_{\text{annihil.}} = 20$, and $\mathcal{N}_{\text{Compt.}} = 320/3$, for $N_f = 2$. In the case of $N_f = 3$, those numbers become $\mathcal{N}_{\text{annihil.}} = 24$, and $\mathcal{N}_{\text{Compt.}} = 384/3$. Calculations of the photon production rate from these channels were done in Ref. [32], an evaluation with general anisotropic distribution functions (not limited to small deviations

from equilibrium) appeared in Ref. [33], and a viscosity-corrected rate (to first order in δf) was obtained recently in [34], assuming forward-scattering dominance of the photon-producing reaction. The rates reported here are obtained through a numerical integration of Eq. (8) with out-of-equilibrium distribution functions (Eq. (7)). The integrations span the entire accessible phase space, carefully avoiding divergences as prescribed in Ref. [32]. Appropriate quantum statistics have been used.

B. Photon emission from the hadronic gas

As the ensemble of partons thermalizes (totally or partially) and then expands and cools, it hadronizes into an ensemble of colorless hadrons called here the hadronic gas (HG) which continues to expand and to cool even more. The HG thermal electromagnetic emissivity has been characterized in Ref. [35]. Following that reference, a Massive Yang-Mills (MYM) model is used to model the interactions between light pseudoscalars, vector and axial vector mesons. The set we consider contains the elements $\{\pi, K, \rho, K^*, a_1\}$, and the most important photon-producing rates are $\pi + \rho \to \pi + \gamma$, $\pi + \pi \to \rho + \gamma$, $\pi + K^* \to K + \gamma$, $\pi + K \to K^* + \gamma$, $\rho + K \to K + \gamma$, $K^* + K \to \pi + \gamma$. Two-body photon-production processes dominate the phase space for photon transverse momenta above 0.5 GeV [35]. All isospin-allowed channels are considered.

The viscous corrections also demand a complete recalculation of the HG photon rates, by including the corrected distribution functions - see Eq. (7) - in all the relevant rate equations. Note that corrections of order δf^2 are neglected for consistency, as are corrections to Pauli-blocking or Bose-enhancement effects. These corrections are found to be small. The Appendix outlines the procedure for correcting the electromagnetic emissivities, allowing for viscous effects in the hadronic distribution functions.

IV. RESULTS

A. Viscous corrections: generalities

For both cases discussed in the previous section (QGP and HG), rates for "viscous photons" were not shown. In fact, those require detailed dynamical information as they depend on the details of $\pi^{\mu\nu}$ and of its time evolution as specified by Eqs. (7) and (5). It is thus appropriate to examine this quantity here, and this is done in Figure 4, in
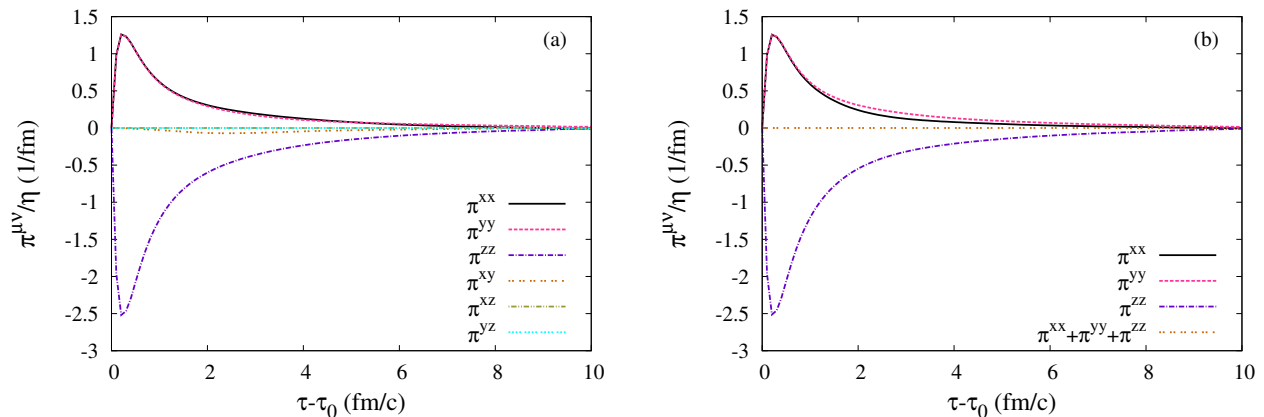

FIG. 4. (Color online) Left panel: The time evolution of different components of the local $\pi^{\mu\nu}$ tensor, divided by η. Right panel: The time evolution of the diagonal elements of π^{ij} (scaled by η), and also that of the trace of the viscous tensor. The calculations are done for a fluid cell at $x = y = 2.5$ fm, and $z = 0$, and the impact parameter is $b = 4.47$ fm.

the rest frame of a fluid cell; note that there π^{tt} is 0. At the initial time, the viscous corrections are non-existent, as we initialize the viscous pressure tensor to zero. They build up quickly, and then decay back to zero. Right after the initial time, the magnitude of the zz component is larger than the other two diagonal ones by roughly a factor of 2, and this fact persists up to late times. The relative sign of π_{zz} can be understood from the fact that π_{ij} should be traceless in the fluid rest frame (c.f. Eqs. (5, 6)). Note that this requirement was not enforced explicitly at each step of the calculation. The preservation of this trace then reflects the stability of the numerics: see the right panel

of Figure 4. The slight difference between π_{xx} and π_{yy} is to be expected because of the elliptic shape of the system: the $x - y$ symmetry is broken by the finite impact parameter.
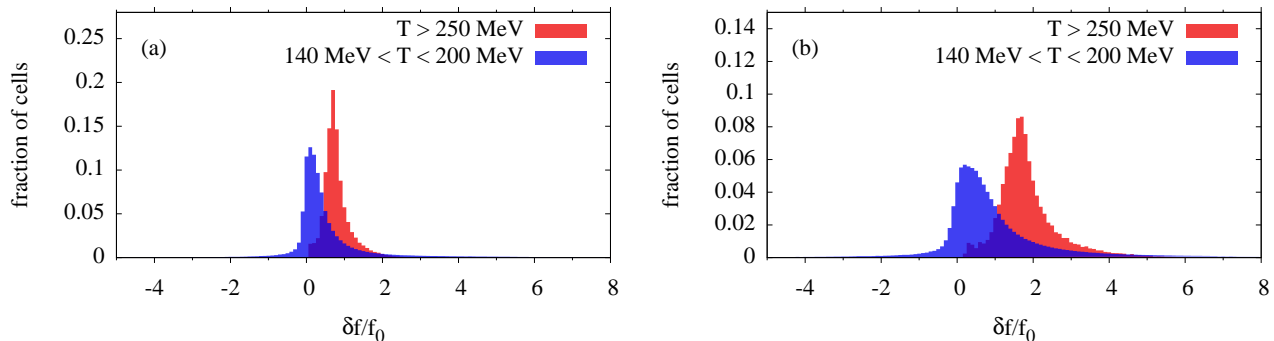

FIG. 5. (Color online) The fraction of $\eta_s \approx 0$ fluid cells with a certain value of $\delta f/f_0$, for different values of the photon momentum in the nucleus-nucleus center of mass frame: 2 GeV (left panel), and 3 GeV (right panel). The range of temperature $T > 250$ MeV corresponds to $\tau - \tau_0 \lesssim 2$ fm/c.

To get a qualitative picture and develop some intuition for the importance of the viscous corrections, the following procedure was implemented. In the nucleus-nucleus center of mass frame, one picks a photon momentum in the $x - y$ plane, at an angle of $\pi/4$. The z axis is the beam axis. Lorentz-transforming to the rest-frame of each fluid cell, the local value of the photon momentum is obtained. Since photons are formed in $2 \to 2$ processes, the magnitude of this momentum is then roughly equal to the magnitude of the momentum of one of the interacting particles. Finally, posing that this particle is a massless fermion will enable a determination of the viscous correction to its distribution function. This study is restricted to a slice in space-time rapidity, η_s, centered around 0. This procedure is clearly approximate - not all particles are massless and not all are fermions - but should nevertheless produce a result indicative of the physics at play. Defining bins of size 0.1 in the relative variable $\delta f/f_0$, the fraction of $\eta_s \approx 0$ cells with a certain value of this relative variable is plotted in Figure 5. In addition, in this study we concentrate on two ranges of temperature: one corresponding to "early times", and another corresponding to "late times" according to Figure 1. The photon energies chosen are typical values of the photon spectrum, see the next subsection. For a photon energy of 2 GeV, one sees that $\approx 20\%$ of the fluid cells have a $\delta f/f_0 \geq 1$, at early times, and that the distribution around this value is fairly narrow. For a higher photon energy of 3 GeV, this distribution has grown in width, now with 80% of the high-temperature cells with $\delta f/f_0 \geq 1$ and $\approx 30\%$ of them with $\delta f/f_0 \geq 2$: a clear violation of the perturbative nature of the approximation. In a given panel of Figure 5, the amount of larger viscous corrections at higher temperatures can be understood: those cases correspond to situations at early times where the elements of the $\pi^{\mu\nu}$ tensor are large (see Figure (4)). Higher momenta will command larger viscous corrections, see Eq. (7), and hence the broadening of the distributions for a given range in T when going from the left to the right panel of Figure 5. Note that repeating the lower temperature part of this analysis by assuming that the corrected particles are massive π's or even massive ρ's do not change its conclusions. A negligible but non-zero number of high-momentum cells have $\delta f/f_0 \leq -1$. For those cells the photon emission probability has been set to zero. What emerges here is an explicit message of caution. In contrast to hadron calculations where only properties at the freeze-out surface are required, the evaluation of electromagnetic signals requires the *entire* time evolution to be monitored. In the case of the analysis shown here, one should also keep in mind that thermal photons with an energy equal to, or greater than, 3 GeV will lie below those from other sources like the direct photons from primordial nucleon-nucleon collisions, for example [36, 37].

One now proceeds to the evaluation of photon characteristics, and of the influence of viscous effects on them. All of the calculation results shown in the next sections will rely on the use of Averaged Initial Conditions (AICs). A discussion of the effects of Fluctuating Initial Conditions (FICs) on real photons first appears in section IV D.

B. Photon spectrum

As mentioned previously, the measured photon spectrum receives contributions from all times and all phases spanned by the collision dynamics. There are treated in turn here, for pedagogical purposes. The photons originating solely from the QGP phase are first shown in Figure 6, and they are obtained by integrating the rate in Eqs. (8) and (A.26) throughout the time evolution dictated by MUSIC.
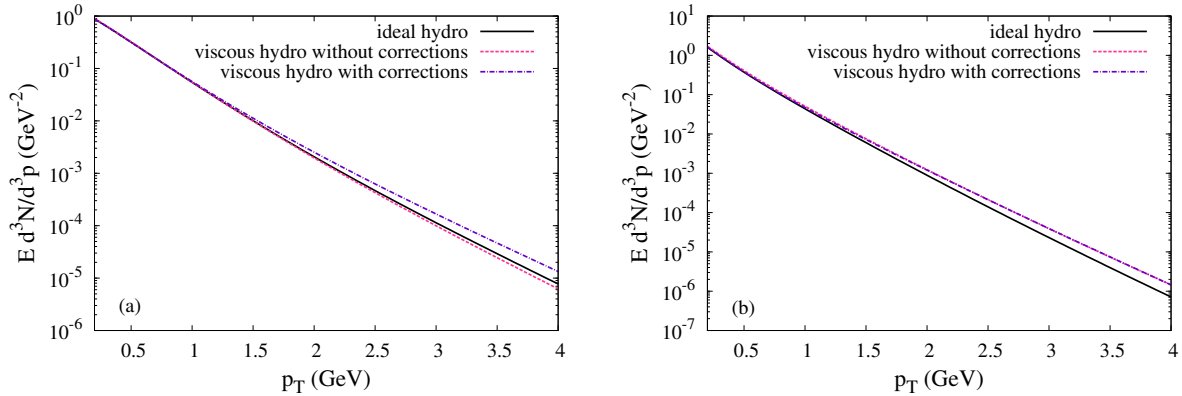
FIG. 6. (Color online) Left panel: The photon yield originating from the phase with parton degrees of freedom only. The contribution from ideal hydro is shown (solid curve), together with the result of using a time evolution associated with viscous hydrodynamics (dotted line), and using a viscous time evolution and corrected microscopic distribution functions (dash-dotted line). Right panel: The photon yield originating from the hadronic gas only. The meaning of the different curves is the same as that in the left panel.

As compared to an ideal hydrodynamical evolution, the viscous evolution starts with a lower initial temperature when the system is entirely in its QGP phase (see Figure 1). Therefore, integrating the QGP photon rates with a viscous hydrodynamic evolution alone produces a photon spectrum slightly lower at high values of p_T than that generated by the ideal hydro. This is the dotted line in Figure 6. Then, using the corrected distribution functions make the photon spectrum harder, as the correction grows as a function of momentum. This is the upper curve in the same figure. The hardening of the QGP photon spectra owing to shear viscous effects had also been noticed in previous work [34, 38, 39].

Turning now to photons originating solely from the HG sector, the relevant spectrum is shown in the right panel of Figure 6. Interestingly, the spectrum with the viscous corrections (viscous hydro and corrected distribution functions) is essentially undistinguishable from that obtained using ideal rates integrated with a viscous time evolution. This can be understood by considering the fact that photons from the HG are emitted later in time, essentially when $\pi^{\mu\nu} \sim 0$, as is made clear in Figure 4. The effect of viscosity are manifested in a slightly harder spectrum: in part a consequence of the temperature in the viscous evolution remaining higher than that in the ideal evolution for intermediate and late times, as shown in Figure 1. The yield of real photons from all thermal sources (QGP + HG) is shown in Figure 7, for an ideal hydrodynamic evolution and also for a viscous evolution (viscous hydro and corrected distribution functions). The difference between the two scenarios is actually small at intermediate values of the photon transverse momentum, growing to being approximately 100% at $p_T = 4$ GeV. At that energy however, the purely thermal photons will lie below other sources and will be sub-dominant, as mentioned already. One may thus conclude here that extracting information about the shear viscosity from photon spectra alone will be an arduous task. More work is needed however to include *all* the photon sources in a theoretically consistent way, with all the viscous corrections.

C. Photon elliptic flow

The flow characteristics of hadrons have contributed considerably to quantify the details of the underlying hydrodynamics, and this fact has been hailed as one of the major milestones of the RHIC program. As for photons, their elliptic flow holds the potential of providing more insight into the dynamics of heavy ion collisions, and into the phase structure of QCD. Indeed, the shape of the real photon v_2 coefficient is directly sensitive to the nature of the underlying degrees of freedom [40], unlike the single-photon spectra of the previous section. The elliptic flow of photons originating solely from the QGP is shown in Figure 8. If one neglects the correction to the distribution functions, the elliptic flow from the viscous evolution appears slightly larger than in the ideal case, reflecting an increase in the azimuthal asymmetry of the fluid flow pattern due to viscosity, consistent with the large gradients at early times implied by Figure 4. However, the corrections to the distribution functions dominate, and make the net anisotropy even smaller than in the ideal case. This behaviour is consistent with the results of Ref. [39]. It is also worthwhile to point out that the apparently negative values of v_2 at very low momenta for photons in the QGP are obtained only using the photon-production rates corresponding to Figure 2. The complete rates of Ref. [31] do not yield negative photon elliptic flow in ideal hydrodynamics. The negative values also appear in earlier calculations [34, 39]. The HG
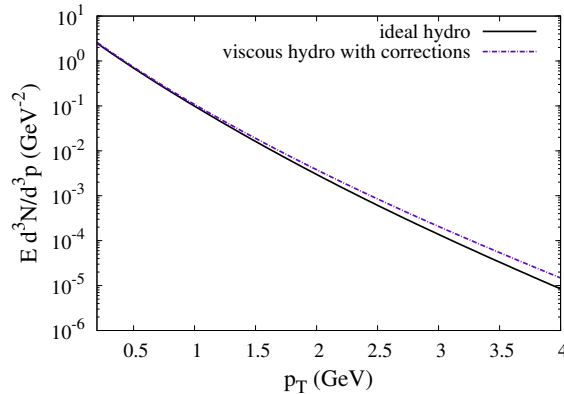
FIG. 7. (Color online) The net thermal photon yield, from QGP and HG sources. The ideal spectrum (i.e. using an ideal hydrodynamics background), and the viscous spectrum (using a viscous hydrodynamics background and corrected microscopic distribution functions) are shown as a solid and dotted line, respectively.
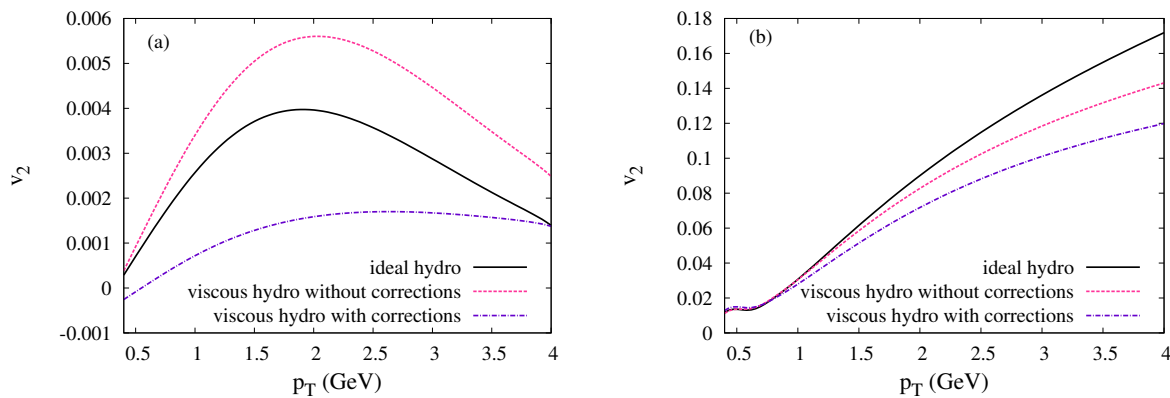

FIG. 8. (Color online) Left panel: The thermal photon elliptic flow, considering only the photons originating from the QGP. As in previous figures, the results of using ideal hydrodynamics (solid line), viscous hydrodynamics with equilibrium rates (dotted line), and viscous hydrodynamics with δf corrections (dash-dotted line) are shown separately. Right panel: The thermal photon elliptic flow, considering only the photons originating from the HG. The lines have the same meaning as those in the left panel.

v_2 is shown in the right panel of Figure 8 and there, all viscous corrections make the elliptic flow smaller, unlike the case for the QGP. This is again a reflection of the richness of the dynamics contained in the time-dependence of $\pi^{\mu\nu}$. Further note that the small structure at low momenta signals a crossover between two different hadronic channels [40]. The net photon v_2 is then calculated and shown in Figure 9. Importantly, the total v_2 is a weighted average of the individual (QGP, and HG) coefficients, the weight being the value of the appropriate single-photon distribution. Hence, in the computation of the final v_2, the small QGP v_2 will get multiplied by a large emission rate, whereas the smaller emission rate of the HG phase gets partially compensated by the larger flows. Both phases therefore contribute to the final profiles shown in Figure 9.

D. Fluctuating initial conditions (FIC)

The recent years have witnessed a paradigm-shift in the analysis of heavy ion collision data. Up until recently, smooth initial state distributions were mostly used in hydrodynamics analyses of relativistic nuclear collisions. These, together with conservation laws, imply that odd-numbered expansion coefficients in Eq. (1) vanish identically. As discussed in the Introduction, this situation has changed with the work of Ref. [15] linking odd-numbered flow harmonics to initial state fluctuations. The hydrodynamic simulation MUSIC with viscous corrections has recently been modified to include FICs [8]. This has been used to make a prediction for size and momentum dependence of the hadronic v_3 at RHIC. This prediction has been recently confirmed [41]. Here we seek to assess the importance of
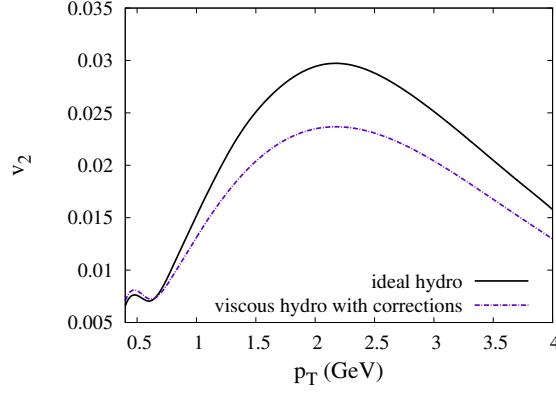
FIG. 9. (Color online) The net thermal photon elliptic flow. The curves have the same meaning as in Figure 7.

the event-by-event fluctuations on photon observables.

For initial conditions that are not smooth, it is important to specify how the reaction plane is determined. The "participant plane" [42] is used here. Namely, one calculates event-by-event the angle ψ_2 with respect to the reaction plane defined by the impact parameter:

$$\psi_2 = \frac{1}{2}\arctan\left(\frac{\langle r^2 \sin(2\phi)\rangle}{\langle r^2 \cos(2\phi)\rangle}\right) \tag{10}$$

where the averages are over wounded nucleon positions, (r, ϕ), in the transverse plane. The angle ψ_2 then goes into the evaluation of v_2, with ψ_2 replacing ψ_r in Eq. (1). Note that the initial eccentricity is maximized by the choice of this participant plane. The studies performed here used ensembles of 50 events, leading to uncertainties of the order of 5% on thermal photon spectra, and of the order of 15% on thermal photon v_2. The precise value of these variations is of course p_T-dependent, but we find that elliptic flow does depend more strongly on the initial structure of the energy density distribution than the momentum spectrum.

As already observed for hadrons [43] and more recently for photons [44], the lumpy initial states lead to a yield enhancement. Again, the QGP and HG contributions are calculated separately. They are shown in the two panels of Figure 10, and the quantitative importance of the enhancement can be judged there. As done previously, only
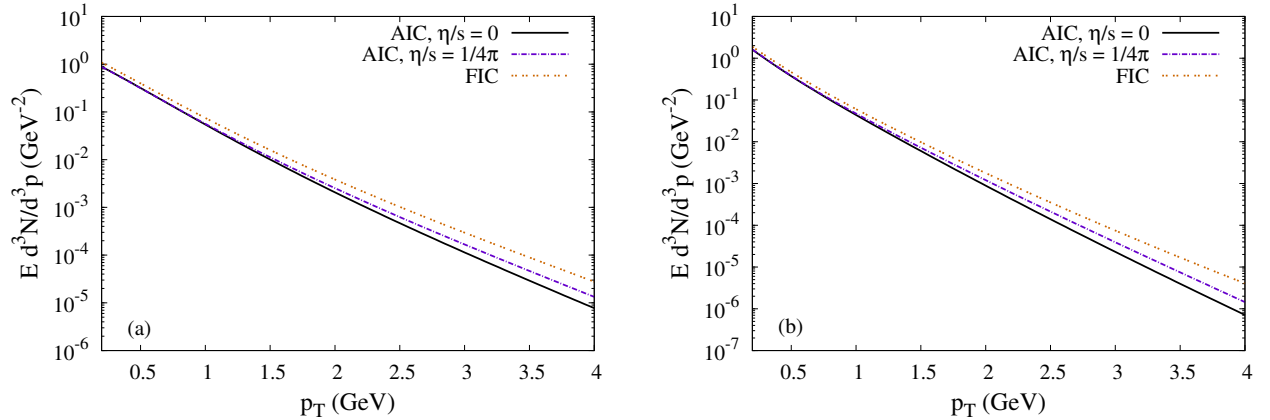

FIG. 10. (Color online) The thermal photon yield, showing the effect of FICs. The left panel shows the contribution from the QGP, the right panel that of the HG. Note that the curve labeled "FIC" also includes all viscous corrections (time evolution and δf)

this time with FICs, we plot the thermal photon v_2 for QGP and HG. This is shown in Figure 11. Finally, the net photon spectrum and v_2 are shown in Figure 12. Clearly, in the centrality range studies in this work, the hot spots and large gradients generated by the fluctuating initial conditions lead to a harder photon spectrum and to a larger elliptic flow, and this remains true with the inclusion of a finite shear viscosity to entropy density ratio.
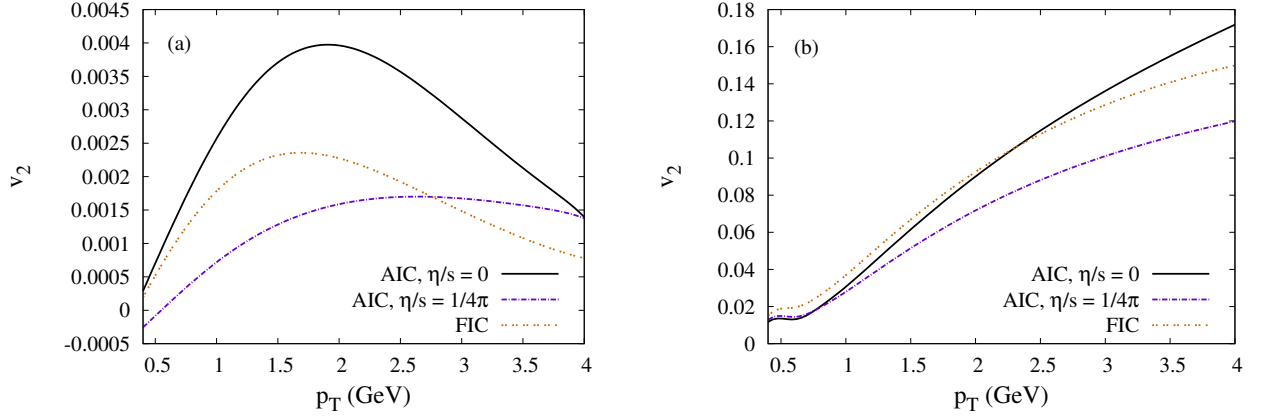
FIG. 11. (Color online) The thermal photon v_2, showing the effect of FICs. The left panel shows the contribution from the QGP, and the right panel that of the HG. Note that the curve labeled "FIC" also includes all viscous corrections (time evolution and δf).
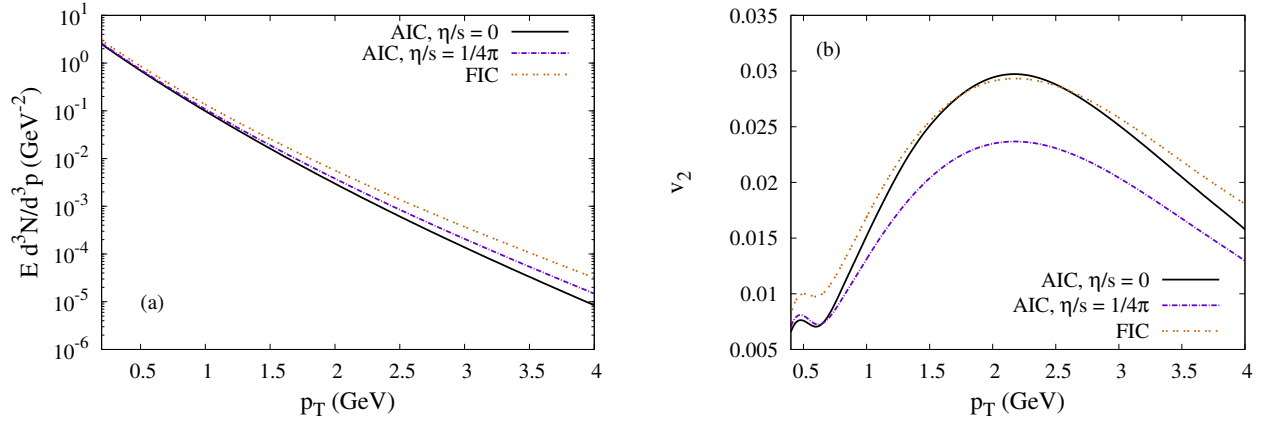

FIG. 12. (Color online) The net thermal photon yield (left panel) and v_2 (right panel), showing the effect of FICs. Note that the curve labeled "FIC" also includes all viscous corrections (time evolution and δf).

V. CONCLUSION

In this work we have sought to establish the quantitative importance of a finite shear viscosity coefficient and of fluctuating initial conditions on two real photon observables: the one-body spectrum and the transverse momentum dependence of the elliptic flow coefficient. This was done using MUSIC, a realistic 3+1D relativistic hydrodynamical simulation. Importantly, comparisons between cases with and without viscous corrections were done using conditions tuned to hadronic experimental data, and this was the case also for studies involving FICs. Results obtained here show that the combined effects of the viscosity and of the FICs are large enough to make their inclusion mandatory in any attempt to quantitatively extract transport coefficients of the hot and dense matter from thermal photon data. It was not the point of this work to explicitly compare with experimental measurements just yet. Firstly, 3+1D relativistic viscous hydrodynamics models are in their infancy, and systematic studies of *all* parameter dependences, in the spirit of that in Ref. [45] for example, will be useful to establish a more precise quantitative link between observables and the underlying hydrodynamics. Secondly, in what concerns the photon sources, an inclusive and consistent treatment of all of them (pQCD photons, photons from jets interacting and fragmenting while losing energy . . .) with and without viscosity is still to be done. Finally, exploring the consequences of what has been found here on electromagnetic observables at the LHC should prove interesting and relevant.

In closing, it is worth mentioning that recently the PHENIX collaboration at RHIC has extracted a direct photon v_2 from measured data [46]. Interestingly, this analysis concludes that the direct photon elliptic flow is comparable in magnitude to that of the π^0. This large photon elliptic flow is a challenge to most approaches, but may contain

some clues about early dynamics prior to hadronic freeze-out [47]. However, a complete theoretical analysis including all that is known in the literature about the production of direct photons in relativistic heavy ion collisions (viscous effects, FICs, the effect of realistic 3+1D hydrodynamical modelling, hadronic chemical potentials, primordial flow) is needed before a more precise assessment can be obtained.

Appendix: Viscous photon rates

Our starting point for the photon emission rate of a $(1 + 2 \to 3 + \gamma)$ process is the expression leading to Eq. (8):

$$
\begin{aligned}
E\frac{d^3R}{d^3p} = \int & \frac{d^3p_1}{2E_1(2\pi)^3}\frac{d^3p_2}{2E_2(2\pi)^3}\frac{d^3p_3}{2E_3(2\pi)^3}\frac{2\pi}{2}|\mathcal{M}|^2 \\
& \times \delta^4(p_1 + p_2 - p_3 - p)f(p_1)f(p_2)\left(1 + f(p_3)\right)
\end{aligned}
\tag{A.1}
$$

The subscripts 1,2 and 3 refer to the two incoming particles and the outgoing particle (not the photon) respectively. Notice that the momentum distribution functions depend on the four-momentum and not only on the zero component (the energy). This can be written as (with $s = (p_1 + p_2)^2, t = (p_2 - p)^2, u = -s - t + m_1^2 + m_2^2 + m_3^2$)

$$
\begin{aligned}
E\frac{d^3R}{d^3p} = & \frac{1}{2^5(2\pi)^8E^2}\int_{s^{\min}}^{\infty}ds\int_{t^{\min}}^{t^{\max}}dt\int_{E_1^{\min}}^{\infty}dE_1\int_{E_2^{\min}}^{E_2^{\max}}dE_2\int_0^{2\pi}d\phi_1\int_0^{2\pi}d\phi_2|\mathcal{M}|^2 \\
& \delta(s - m_1^2 - m_2^2 - 2E_1E_2 + 2|p_1||p_2|\cos\theta)f(p_1)f(p_2)(1 + f(p_1 + p_2 - p))
\end{aligned}
\tag{A.2}
$$

where

$$
\cos\theta = \cos\theta_1\cos\theta_2 + \sin\theta_1\sin\theta_2\cos(\phi_2 - \phi_1)
$$
$$
\cos\theta_1 = \frac{-t - s + m_2^2 + m_3^2 + 2EE_1}{2E|\vec{p}_1|}, \quad \cos\theta_2 = \frac{-t - m_2^2 + 2EE_2}{2E|\vec{p}_2|}
\tag{A.3}
$$

The θ angles represent the angle between a particle's three momentum and the photon's. In other words,

$$
\vec{p}_a \cdot \vec{p}_\gamma = |\vec{p}_a||\vec{p}_\gamma|\cos\theta_a
\tag{A.4}
$$

The ϕ angles represent the azimuthal angles of the incoming particle's direction around the photon's direction. The integration boundaries are given by

$$
s^{\min} \geq (m_1 + m_2)^2, \quad s^{\min} \geq m_3^2
\tag{A.5}
$$

$$
\begin{aligned}
t^{\min(\max)} = & m_1^2 + m_3^2 - \frac{1}{2}\left(\frac{s + m_1^2 - m_2^2}{\sqrt{s}}\right)\left(\frac{s + m_3^2}{\sqrt{s}}\right) \\
& -(+)\sqrt{\frac{(s + m_1^2 - m_2^2)^2 - 4sm_1^2}{s}}\left(\frac{s - m_3^2}{2\sqrt{s}}\right)
\end{aligned}
\tag{A.6}
$$

$$
E_1^{\min} = \frac{Em_1^2}{m_1^2 - u} + \frac{m_1^2 - u}{4E}
\tag{A.7}
$$

$$
\frac{-b + \sqrt{b^2 - ac}}{a} \leq E_2 \leq \frac{-b - \sqrt{b^2 - ac}}{a} \quad (a \text{ is negative})
\tag{A.8}
$$

The a, b and c coefficients are given below. Now, we can take care of the ϕ_2 integration with the Dirac delta. Its roots are

$$\phi_\pm = \phi_1 \pm \cos^{-1}\left(\frac{-s + m_1^2 + m_2^2 + 2E_1 E_2 - 2|\vec{p}_1||\vec{p}_2|\cos\theta_1\cos\theta_2}{2|\vec{p}_1||\vec{p}_2|\sin\theta_1\sin\theta_2}\right) \tag{A.9}$$

However, now we need to keep in mind that where we had $f(E_2)$ for the ideal (no viscous corrections) case, we now have $f(E_2, \theta_2, \phi_2)$, so the ϕ_2 integration goes like

$$\int_0^{2\pi} d\phi_2 \delta(s - m_1^2 - m_2^2 - 2E_1 E_2 + 2|p_1||p_2|\cos\theta)f(E_2, \theta_2, \phi_2) =$$

$$\int_0^{2\pi} d\phi_2 \sum_{j=\pm} \frac{\delta(\phi_2 - \phi_j)f(E_2,\theta_2,\phi_2)}{2|\vec{p}_1||\vec{p}_2|\sin\theta_1\sin\theta_2\sin(\phi_j - \phi_1)} =$$

$$\frac{1}{2|\vec{p}_1||\vec{p}_2|\sin\theta_1\sin\theta_2}\left(\frac{f(E_2,\theta_2,\phi_+)}{\sqrt{1 - \cos^2(\phi_+ - \phi_1)}} + \frac{f(E_2,\theta_2,\phi_-)}{\sqrt{1 - \cos^2(\phi_- - \phi_1)}}\right) =$$

$$\frac{1}{2|\vec{p}_1||\vec{p}_2|\sin\theta_1\sin\theta_2}\frac{1}{\sqrt{1 - \cos^2(\phi_+ - \phi_1)}}\Big(f(E_2,\theta_2,\phi_+) + f(E_2,\theta_2,\phi_-)\Big) =$$

$$\frac{E}{\sqrt{aE_2^2 + 2bE_2 + c}}\Big(f(E_2,\theta_2,\phi_+) + f(E_2,\theta_2,\phi_-)\Big) \tag{A.10}$$

where the a, b and c coefficients are given by

$$
\begin{aligned}
a &= -(s + t - m_2^2 - m_2^3)^2 \\
b &= E\big((s + t - m_2^2 - m_2^3)(s - m_1^2 - m - 2^2) - 2m_1^2(m_2^2 - t)\big) \\
&\quad + E_1(m_2^2 - t)(s + t - m_2^2 - m_2^3) \\
c &= c_2 E_1^2 + c_1 E_1 + c_0 \\
c_2 &= -(t - m_2^2)^2 \\
c_1 &= -2E\big(2m_2^2(s + t - m_1^2 - m_2^2) - (m_2^2 - t)(s - m_1^2 - m_2^2)\big) \\
c_0 &= 4E^2 m_1^2 m_2^2 + m_2^2(s + t - m_2^2 - m_2^3) + m_1^2(m_2^2 - t)^2 - E^2(s - m_1^2 - m_2^2)^2 \\
&\quad + (s - m_1^2 - m_2^2)(t - m_2^2)(s + t - m_2^2 - m_2^3)
\end{aligned}
\tag{A.11}
$$

So at this point, the rate is given by

$$E\frac{d^3R}{d^3p} = \frac{1}{32(2\pi)^8 E}\int_{s^{\min}}^{\infty} ds \int_{t^{\min}}^{t^{\max}} dt \int_{E_1^{\min}}^{\infty} dE_1 \int_{E_2^{\min}}^{E_2^{\max}} dE_2 \int_0^{2\pi} d\phi_1 |\mathcal{M}|^2 f(E_1,\theta_1,\phi_1)$$

$$\Big(f(E_2,\theta_2,\phi_+) + f(E_2,\theta_2,\phi_-)\Big)(1 + f(E_1 + E_2 - E))\frac{1}{\sqrt{aE_2^2 + 2bE_2 + c}} \tag{A.12}$$

We have not corrected the distribution functions for the outgoing particle (Pauli blocking or Bose enhancement). At this point, we look more carefully at the form of the correction (choosing Bose enhancement for illustrative purposes):

$$f(p_a) = f_0(E_a) + \delta f(p_a) = f_0(E_a) + \left(\frac{\eta}{s}\frac{1}{2T^3}f_0(E_a)\big(1 + f_0(E_a)\big)p_a^\alpha p_a^\beta \frac{\pi_{\alpha\beta}}{\eta}\right) \tag{A.13}$$

One needs to properly express p^α in terms of integration variables. Because the incoming particles angles are given with respect to the photon's direction, the angles of the photon (in the fluid frame) will explicitly appear in the expressions for the particles four momentum. The zero component of p^α is just the energy, so the interesting parts are the 1,2 and 3 components. In what follows, the subscript a will refer to the incoming particles (1 or 2), and the subscript γ will denote angles for the photon. The photon angles are given with respect to the local frame of each fluid cell. Note that even if we use the ϕ_a notation, ϕ_2 is still given by equation (A.9). Also, all 3-vectors in the following expressions are unitary vectors. The photon's direction is given by

$$\vec{p_\gamma} = (\sin\theta_\gamma \cos\phi_\gamma, \sin\theta_\gamma \sin\phi_\gamma, \cos\theta_\gamma) \tag{A.14}$$

We need to specify the origin for ϕ_a ($\phi_a = 0$). Since the ϕ_a integration is over 2π, the origin is arbitrary. Let's choose the origin to be in the z-p_γ plane. Then,

$$\vec{p_a}(\phi_a = 0) = \left(\sin(\theta_\gamma - \theta_a)\cos\phi_\gamma, \sin(\theta_\gamma - \theta_a)\sin\phi_\gamma, \cos(\theta_\gamma - \theta_a) \right)$$
$$= \big((\sin\theta_\gamma\cos\theta_a - \cos\theta_\gamma\sin\theta_a)\cos\phi_\gamma,$$
$$(\sin\theta_\gamma\cos\theta_a - \cos\theta_\gamma\sin\theta_a)\sin\phi_\gamma, \cos\theta_\gamma\cos\theta_a + \sin\theta_\gamma\sin\theta_a \big) \tag{A.15}$$

To have an expression for $\vec{p_a}$, we need to rotate $\vec{p_a}(\phi_a = 0)$ by an angle of ϕ_a around $\vec{p_\gamma}$. The rotation matrix is then given by

$$R = \begin{pmatrix} r_{11} & r_{12} & r_{13} \\ r_{21} & r_{22} & r_{23} \\ r_{31} & r_{32} & r_{33} \end{pmatrix} \tag{A.16}$$

$$r_{11} = \cos\phi_a + \sin^2\theta_\gamma\cos^2\phi_\gamma(1 - \cos\phi_a)$$
$$r_{12} = \sin^2\theta_\gamma\cos\phi_\gamma\sin\phi_\gamma(1 - \cos\phi_a) - \cos\theta_\gamma\sin\phi_a$$
$$r_{13} = \sin\theta_\gamma\cos\theta_\gamma\cos\phi_\gamma(1 - \cos\phi_a) + \sin\theta_\gamma\sin\phi_\gamma\sin\phi_a$$
$$r_{21} = \sin^2\theta_\gamma\cos\phi_\gamma\sin\phi_\gamma(1 - \cos\phi_a) + \cos\theta_\gamma\sin\phi_a$$
$$r_{22} = \cos\phi_a + \sin^2\theta_\gamma\sin^2\phi_\gamma(1 - \cos\phi_a)$$
$$r_{23} = \sin\theta_\gamma\cos\theta_\gamma\sin\phi_\gamma(1 - \cos\phi_a) - \sin\theta_\gamma\cos\phi_\gamma\sin\phi_a$$
$$r_{31} = \sin\theta_\gamma\cos\theta_\gamma\cos\phi_\gamma(1 - \cos\phi_a) - \sin\theta_\gamma\sin\phi_\gamma\sin\phi_a$$
$$r_{32} = \sin\theta_\gamma\cos\theta_\gamma\sin\phi_\gamma(1 - \cos\phi_a) + \sin\theta_\gamma\cos\phi_\gamma\sin\phi_a$$
$$r_{33} = \cos\phi_a + \cos^2\theta_\gamma(1 - \cos\phi_a) \tag{A.17}$$

So our expression for $\vec{p_a}$ is finally

$$\begin{bmatrix} p_a^x \\ p_a^y \\ p_a^z \end{bmatrix} = R \begin{bmatrix} (\sin\theta_\gamma\cos\theta_a - \cos\theta_\gamma\sin\theta_a)\cos\phi_\gamma \\ (\sin\theta_\gamma\cos\theta_a - \cos\theta_\gamma\sin\theta_a)\sin\phi_\gamma \\ \cos\theta_\gamma\cos\theta_a + \sin\theta_\gamma\sin\theta_a \end{bmatrix} \tag{A.18}$$

Note that all the components of p_a are proportional to either one or no power of $\cos\theta_a$, $\sin\theta_a$, $\cos\phi_a$ and $\sin\phi_a$, so we can rewrite, for instance, the x component as (with the A,B and C coefficients that only depend on photon angles)

$$p_a^x = \cos\theta_a\left\{ \cos\phi_a A_x^c + \sin\phi_a B_x^c + C_x^c \right\} + \sin\theta_a\left\{ \cos\phi_a A_x^s + \sin\phi_a B_x^s + C_x^s \right\} \tag{A.19}$$

and in a similar way we have

$$p_a^y = \cos\theta_a\left\{ \cos\phi_a A_y^c + \sin\phi_a B_y^c + C_y^c \right\} + \sin\theta_a\left\{ \cos\phi_a A_y^s + \sin\phi_a B_y^s + C_y^s \right\} \tag{A.20}$$

$$p_a^z = \cos\theta_a\left\{ \cos\phi_a A_z^c + \sin\phi_a B_z^c + C_z^c \right\} + \sin\theta_a\left\{ \cos\phi_a A_z^s + \sin\phi_a B_z^s + C_z^s \right\} \tag{A.21}$$

Now, going back to the expression for the rate, only the viscous corrected momentum distribution functions actually depend on ϕ_1 so let's look at the ϕ_1 integration of the viscous corrections

$$\int_0^{2\pi} d\phi_1 \Big(f_0(E_1) + \delta f(p_1) \Big)\Big(f_0(E_2) + \delta f(p_2) \Big)$$
$$\approx \int_0^{2\pi} d\phi_1 f_0(E_1)f_0(E_2) + f_0(E_1)\delta f(p_2) + f_0(E_2)\delta f(p_1) \tag{A.22}$$

where the term proportional to $\delta f(p_1)\delta f(p_2)$ has been neglected. Since $f_0(E_a)$ is independent of ϕ_a, what we really need to look at is

$$\int_0^{2\pi} d\phi_1 \delta f(p_a) \propto \int_0^{2\pi} d\phi_1 p_a^\alpha p_a^\beta \frac{\pi_{\alpha\beta}}{\eta} \tag{A.23}$$

It should be pointed out that ϕ_2 (which is given by ϕ_+ or ϕ_-) differs from ϕ_1 by a term which, as far as the integration over ϕ_1 is concerned, is a constant. Because the only dependance on ϕ_2 comes from sine or cosine terms, and because the ϕ_1 integration is over a full cycle (from 0 to 2π), ϕ_2 is actually the same as ϕ_1. Or, more precisely,

$$\int_0^{2\pi} d\phi_1 f(\cos\phi_1, \sin\phi_1) = \int_0^{2\pi} d\phi_1 f(\cos\phi_2, \sin\phi_2)$$

$$= \int_0^{2\pi} d\phi_1 f(\cos\phi_+, \sin\phi_+) = \int_0^{2\pi} d\phi_1 f(\cos\phi_-, \sin\phi_-) \quad \text{(A.24)}$$

One can replace the $\left(f(E_2, \theta_2, \phi_+) + f(E_2, \theta_2, \phi_-)\right)$ term in (A.10) by $2f(E_2, \theta_2, \phi_1)$. Furthermore, the ϕ_1 integration will then be treated the same way regardless of the particle being considered (1 or 2). Considering, for instance, the $p_1^x p_1^y$ term and carrying out the ϕ_1 integration, one obtains

$$\int_0^{2\pi} d\phi_1 p_1^x p_1^y = \int_0^{2\pi} d\phi_1 \Big(\cos\theta_1 \big\{ \cos\phi_1 A_x^c + \sin\phi_a B_x^c + C_x^c \big\} + \sin\theta_1 \big\{ \cos\phi_1 A_x^s + \sin\phi_1 B_x^s + C_x^s \big\} \Big)$$

$$\Big(\cos\theta_1 \big\{ \cos\phi_1 A_y^c + \sin\phi_1 B_y^c + C_y^c \big\} + \sin\theta_1 \big\{ \cos\phi_1 A_y^s + \sin\phi_1 B_y^s + C_y^s \big\} \Big)$$

$$= \pi \Big[\cos^2\theta_1 \Big(A_x^c A_y^c + B_x^c B_y^c + 2C_x^c C_y^c \Big) + \sin^2\theta_1 \Big(A_x^s A_y^s + B_x^s B_y^s + 2C_x^s C_y^s \Big)$$

$$+ \cos\theta_1 \sin\theta_1 \Big(A_x^c A_y^s + B_x^c B_y^s + 2C_x^c C_y^s + A_x^s A_y^c + B_x^s B_y^c + 2C_x^s C_y^c \Big) \Big] \quad \text{(A.25)}$$

If we were dealing with particle 2, the θ_1's would be θ_2's, and if we were looking at other x-y-z combinations the A,B and C coefficients would be different, but the general form is always the same. The important thing is that, after the ϕ_1 integration, the $p_a^\alpha p_a^\beta$ terms can easily be split into a part that depends only on E and T, the photon energy and the local temperature (via the $\cos\theta_a$ and $\sin\theta_a$), and one that depends only on the photon angles (the A,B and C coefficients). So in the end, the photon production rate, including momentum distribution function modifications from viscosity, is given by

$$E\frac{d^3R}{d^3p} = \frac{1}{16(2\pi)^8 E} \int_{s^{\min}}^{\infty} ds \int_{t^{\min}}^{t^{\max}} dt \int_{E_1^{\min}}^{\infty} dE_1 \int_{E_2^{\min}}^{E_2^{\max}} dE_2 |\mathcal{M}|^2 (1 + f_0(E_1 + E_2 - E))$$

$$\times \frac{1}{\sqrt{aE_2^2 + 2bE_2 + c}} \Big(f_0(E_1)f_0(E_2) + \frac{\eta}{s}\frac{1}{2T^3} \big[f_0(E_2)f_0(E_1)\big(1 + f_0(E_1)\big) p_1^\alpha p_1^\beta$$

$$+ f_0(E_1)f_0(E_2)\big(1 + f_0(E_2)\big) p_2^\alpha p_2^\beta \big] \frac{\pi_{\alpha\beta}}{\eta} \Big) \quad \text{(A.26)}$$

where it is understood that the $p_a^\alpha p_a^\beta$ terms have been integrated over ϕ_1, from 0 to 2π. Now if we substitute Eq. (A.25) (and similar expressions for other $p_a^\alpha p_a^\beta$ combinations) into the above expression, the result can be expressed in terms of four-integrals for which the result depends only on E and T, multiplied by a combination of terms that depend only on θ_γ and ϕ_γ. The integrals that need to be computed are then of the type

$$\int_{s^{\min}}^{\infty} ds \int_{t^{\min}}^{t^{\max}} dt \int_{E_1^{\min}}^{\infty} dE_1 \int_{E_2^{\min}}^{E_2^{\max}} dE_2 |\mathcal{M}|^2 (1 + f_0(E_1 + E_2 - E)) \frac{1}{\sqrt{aE_2^2 + 2bE_2 + c}} [...] \quad \text{(A.27)}$$

where $[...]$ is one of

$$[...] = \begin{cases} f_0(E_1)(E_2^2 - m_2^2)\cos^2\theta_2 f_0(E_2)\big(1 + f_0(E_2)\big) \\[2mm] f_0(E_1)(E_2^2 - m_2^2)\sin^2\theta_2 f_0(E_2)\big(1 + f_0(E_2)\big) \\[2mm] f_0(E_1)(E_2^2 - m_2^2)\cos\theta_2 \sin\theta_2 f_0(E_2)\big(1 + f_0(E_2)\big) \\[2mm] f_0(E_2)(E_1^2 - m_1^2)\cos^2\theta_1 f_0(E_1)\big(1 + f_0(E_1)\big) \\[2mm] f_0(E_2)(E_1^2 - m_1^2)\sin^2\theta_1 f_0(E_1)\big(1 + f_0(E_1)\big) \\[2mm] f_0(E_2)(E_1^2 - m_1^2)\cos\theta_1 \sin\theta_1 f_0(E_1)\big(1 + f_0(E_1)\big) \end{cases} \quad \text{(A.28)}$$

where $(E_a^2 - m_a^2)$ is just $|\vec{p}_a|^2$, which we have omitted in the derivations above. For instance, to compute the contribution to the correction from the $p_1^x p_1^y$ term, one would need the last three terms in Eq. (A.28) (the ones corresponding to $\cos^2\theta_1$, $\sin^2\theta_1$, $\cos\theta_1\sin\theta_1$). Each of these terms, would then be multiplied by some combination of the A, B, and C terms. In this example, the $\cos^2\theta_1$ gets multiplied by $\left(A_x^c A_y^c + B_x^c B_y^c + 2C_x^c C_y^c\right)$, as in Eq. (A.25.)

[1] K. Adcox *et al.* (PHENIX), Nucl. Phys., **A757**, 184 (2005).
[2] J. Adams *et al.* (STAR), Nucl. Phys., **A757**, 102 (2005).
[3] B. B. Back *et al.*, Nucl. Phys., **A757**, 28 (2005).
[4] I. Arsene *et al.* (BRAHMS), Nucl. Phys., **A757**, 1 (2005).
[5] P. F. Kolb and U. W. Heinz, Quark Gluon Plasma 3 ed R C Hwa and X N Wang (Singapore: World Scientific), 634 (2003), arXiv:nucl-th/0305084.
[6] K. Aamodt *et al.* (ALICE), Phys. Rev. Lett., **105**, 252302 (2010); P. Steinberg *et al.* (ATLAS), (2011), arXiv:1107.2182 [nucl-ex].
[7] See, for example, B. Schenke, (2011), arXiv:1106.6012 [nucl-th], and references therein.
[8] B. Schenke, S. Jeon, and C. Gale, Phys. Rev. Lett., **106**, 042301 (2011).
[9] B. Schenke, S. Jeon, and C. Gale, (2011), arXiv:1102.0575 [hep-ph].
[10] C. Shen *et al.*, (2011), arXiv:1106.6350 [nucl-th].
[11] H. Song, S. A. Bass, and U. Heinz, Phys. Rev., **C83**, 054912 (2011).
[12] M. Luzum and P. Romatschke, Phys. Rev., **C78**, 034915 (2008).
[13] P. Romatschke and U. Romatschke, Phys. Rev. Lett., **99**, 172301 (2007).
[14] A. M. Poskanzer and S. A. Voloshin, Phys. Rev., **C58**, 1671 (1998).
[15] B. Alver and G. Roland, Phys. Rev., **C81**, 054905 (2010).
[16] B. Schenke, S. Jeon, and C. Gale, Phys. Rev., **C82**, 014903 (2010).
[17] A. Kurganov and E. Tadmor, Journal of Computational Physics, **160**, 214 (2000).
[18] P. Huovinen and P. Petreczky, Nucl. Phys., **A837**, 26 (2010).
[19] W. Israel, Ann. Phys., **100**, 310 (1976).
[20] J. Stewart, Proc.Roy.Soc.Lond., **A357**, 59 (1977).
[21] W. Israel and J. M. Stewart, Ann. Phys., **118**, 341 (1979).
[22] M. Grmela and H. C. Ottinger, Phys. Rev., **E56**, 6620 (1997).
[23] A. Muronga, Phys. Rev. Lett., **88**, 062302 (2002).
[24] R. Baier, P. Romatschke, D. T. Son, A. O. Starinets, and M. A. Stephanov, JHEP, **04**, 100 (2008).
[25] P. Kovtun *et al.*, Phys. Rev. Lett., **94**, 111601 (2005).
[26] M. Mia, K. Dasgupta, C. Gale, and S. Jeon, Nucl. Phys., **B839**, 187 (2010).
[27] A. Buchel, R. C. Myers, and A. Sinha, JHEP, **03**, 084 (2009).
[28] A. Cherman, T. D. Cohen, and P. M. Hohler, JHEP, **02**, 026 (2008).
[29] F. Cooper and G. Frye, Phys. Rev., **D10**, 186 (1974).
[30] K. Dusling, G. D. Moore, and D. Teaney, Phys. Rev., **C81**, 034907 (2010).
[31] P. Arnold, G. D. Moore, and L. G. Yaffe, JHEP, **12**, 009 (2001).
[32] J. I. Kapusta, P. Lichard, and D. Seibert, Phys. Rev., **D44**, 2774 (1991).
[33] B. Schenke and M. Strickland, Phys. Rev., **D76**, 025023 (2007).
[34] K. Dusling, Nucl. Phys., **A839**, 70 (2010).
[35] S. Turbide, R. Rapp, and C. Gale, Phys. Rev., **C69**, 014903 (2004).
[36] S. Turbide, C. Gale, E. Frodermann, and U. Heinz, Phys. Rev., **C77**, 024909 (2008).
[37] G.-Y. Qin, J. Ruppert, C. Gale, S. Jeon, and G. D. Moore, Phys.Rev., **C80**, 054909 (2009).
[38] J. R. Bhatt and V. Sreekanth, Int. J. Mod. Phys., **E19**, 299 (2010); J. R. Bhatt, H. Mishra, and V. Sreekanth, JHEP, **11**, 106 (2010).
[39] A. K. Chaudhuri and B. Sinha, Phys. Rev., **C83**, 034905 (2011).
[40] R. Chatterjee, E. S. Frodermann, U. W. Heinz, and D. K. Srivastava, Phys. Rev. Lett., **96**, 202302 (2006); U. W. Heinz, R. Chatterjee, E. S. Frodermann, C. Gale, and D. K. Srivastava, Nucl. Phys., **A783**, 379 (2007).
[41] A. Adare *et al.* (PHENIX), (2011), arXiv:1105.3928 [nucl-ex].
[42] H. Holopainen, H. Niemi, and K. J. Eskola, Phys.Rev., **C83**, 034901 (2011).
[43] Z. Qiu and U. W. Heinz, Phys. Rev., **C84**, 024911 (2011).
[44] R. Chatterjee, H. Holopainen, T. Renk, and K. J. Eskola, Phys. Rev., **C83**, 054908 (2011).
[45] C. Shen, U. Heinz, P. Huovinen, and H. Song, Phys. Rev., **C82**, 054904 (2010).
[46] A. Adare *et al.* (PHENIX), (2011), arXiv:1105.4126 [nucl-ex].
[47] H. van Hees, C. Gale, and R. Rapp, (2011), arXiv:1108.2131 [hep-ph].